

Real-Data Testing of Distributed Acoustic Sensing for Offshore Earthquake Early Warning

Jiuxun Yin^{*1}, Marcelo A. Soto², Jaime Ramírez³, Valey Kamalov⁴, Weiqiang Zhu¹, Allen Husker¹, and Zhongwen Zhan¹

Abstract

We present a real-data test for offshore earthquake early warning (EEW) with distributed acoustic sensing (DAS) by transforming submarine fiber-optic cable into a dense seismic array. First, we constrain earthquake locations using the arrival-time information recorded by the DAS array. Second, with site effects along the cable calibrated using an independent earthquake, we estimate earthquake magnitudes directly from strain rate amplitudes by applying a scaling relation transferred from onshore DAS arrays. Our results indicate that using this single 50 km offshore DAS array can offer ~3 s improvement in the alert time of EEW compared to onshore seismic stations. Furthermore, we simulate and demonstrate that multiple DAS arrays extending toward the trench placed along the coast can uniformly improve alert times along a subduction zone by more than 5 s.

Cite this article as Yin, J., M. A. Soto, J. Ramírez, V. Kamalov, W. Zhu, A. Husker, and Z. Zhan (2023). Real-Data Testing of Distributed Acoustic Sensing for Offshore Earthquake Early Warning, *The Seismic Record.* **3(4)**, 269–277, doi: 10.1785/0320230018.

Supplemental Material

Introduction

Earthquake early warning (EEW) systems are crucial for mitigating seismic hazards. Current EEW algorithms predominantly rely on seismic data (Allen and Melgar, 2019) and can be classified into three main categories: point-source, finite-fault, and ground-motion-model based. Multiple algorithms and various data types are often integrated into one system to enhance accuracy. For instance, the U.S. Geological Survey (USGS) ShakeAlert system, operational along the west coast of the United States, incorporates both point-source earth-quake point-source integrated code (EPIC; Chung et al., 2019) and finite-fault rupture detector (FinDer; Böse et al., 2012) algorithms (Böse et al., 2015; Kohler et al., 2017, 2020; Chung et al., 2020). Developing additional EEW approaches and incorporating more data types are important for enhancing the system's accuracy and robustness.

A significant challenge of EEW systems is the limited coverage in most offshore regions. For example, the South American subduction zone is among the most seismically active regions. The region experienced the largest $M_{\rm w}$ 9.4–9.6 earthquake in 1960 (Satake and Atwater, 2007), resulting in considerable loss of life and financial damage. The Cascadia subduction zone,

site of the 1700 megathrust earthquake (Satake et al., 1996), poses a significant threat to coastal areas in North America due to the potential for another megathrust earthquake. Even southern California, which is not a subduction zone, has numerous M 6+ offshore faults in close proximity to densely populated cities, representing a critical seismic hazard. Deployment of more seismic stations can be one solution, but it is financially challenging, particularly in offshore areas where installing and maintaining ocean-bottom seismometers is prohibitively expensive. As a result, innovative and cost-effective solutions for offshore EEW are in high demand.

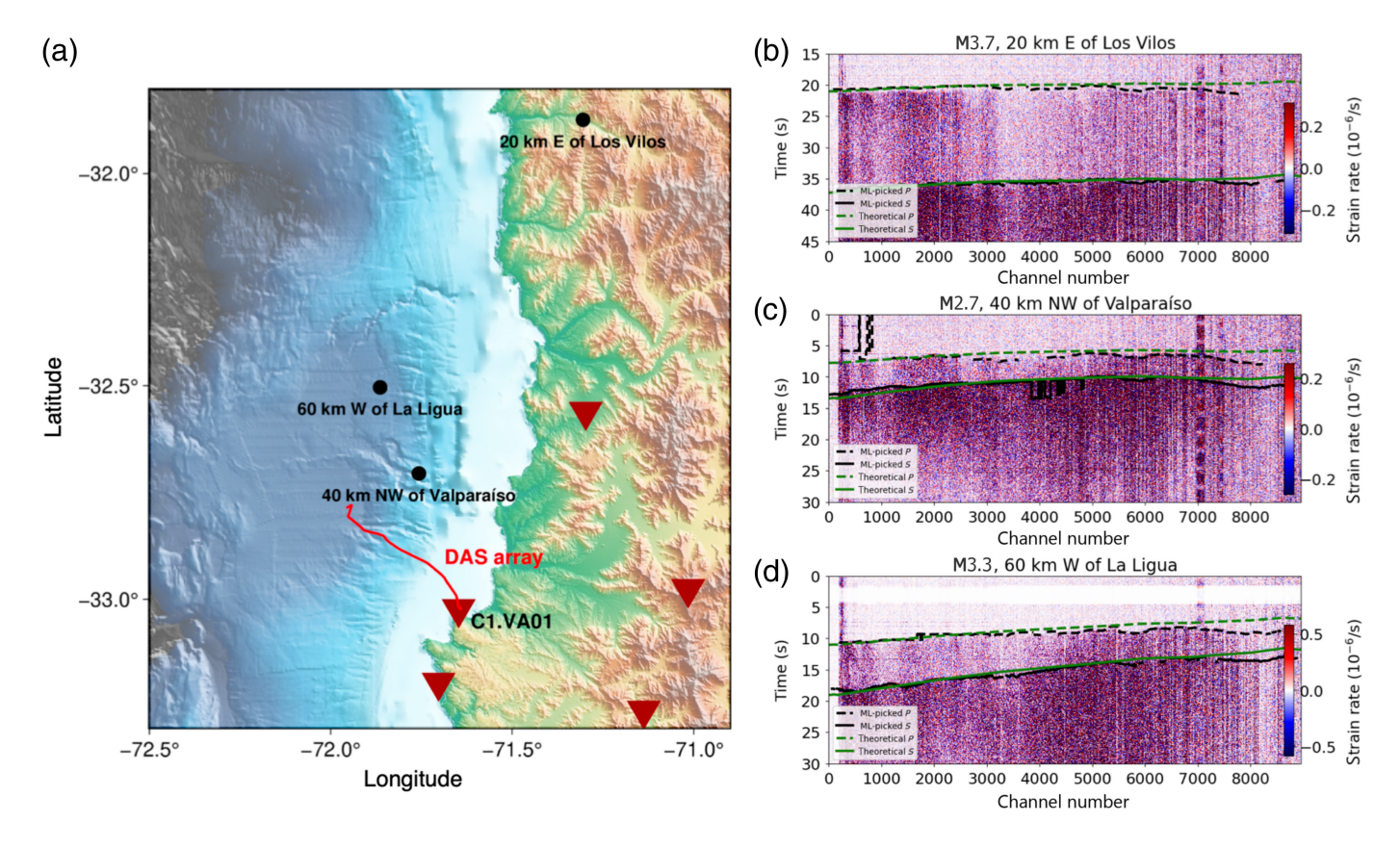
Distributed acoustic sensing (DAS) is an emerging technique with immense potential to augment EEW. It converts

^{1.} Seismological Laboratory, Division of Geological and Planetary Sciences, California Institute of Technology, Pasadena, California, U.S.A., (b) https://orcid.org/0000-0003-0641-5680 (JY); https://orcid.org/0000-0003-1139-0502 (AH); https://orcid.org/0000-0002-5586-2607 (ZZ);

^{2.} Department of Electronics Engineering, Universidad Técnica Federico Santa María, Valparaíso, Chile, (b) https://orcid.org/0000-0002-2140-2012 (MAS); 3. Novelcode SpA, Viña del Mar, Chile; 4. Valey Kamalov LLC, Gainesville, Florida, U.S.A.

^{*}Corresponding author: yinjx@caltech.edu

^{© 2023.} The Authors. This is an open access article distributed under the terms of the CC-BY license, which permits unrestricted use, distribution, and reproduction in any medium, provided the original work is properly cited.



an optical fiber cable into a dense seismic array (Zhan, 2019) and can directly utilize preexisting submarine telecommunication fiber-optic networks in offshore regions (Lindsey et al., 2017; Marra et al., 2022; Shinohara et al., 2022). However, due to the limited availability of submarine cables for DAS applications, there have been very few real-data demonstrations of DAS for offshore EEW. For example, the recent study applied DAS for magnitude estimation and ground-motion prediction in EEW (Lior et al., 2023). Their method involved converting DAS strain to ground acceleration, and combining it with earthquake stress-drop estimation for magnitude estimation and ground-motion prediction. Alternatively, Yin et al. (2023) developed a data-driven scaling relation of DAS amplitude to estimate earthquake magnitude from DAS peak amplitude directly. They also demonstrated that, with minor calibration, the scaling relation developed from terrestrial DAS arrays could be applied to submarine DAS arrays.

In this study, we examine the integration of DAS data into a general EEW workflow. We use data from a submarine cable running from the United States to Chile as a demonstration. Between 10 and 14 June 2022, a DAS interrogator unit was temporarily deployed at the Chilean end, converting the first 50 km of the cable into a DAS system (Fig. 1a). During the

Figure 1. Our study area and earthquakes. (a) Map of the study area in Chile. Red curve is the distributed acoustic sensing (DAS) array. Black dots are the three earthquakes. Dark red triangles are the permanent seismic stations in this area. (b–d) Recorded DAS waveforms of the three earthquakes. Dashed and solid lines correspond to the *P*- and *S*-wave pickings, respectively. The green color lines are the theoretical arrivals from IASP91 velocity model. The black lines are the phase picking from PhaseNet-DAS (Yin et al., 2023; Zhu et al., 2023).

four-day measurement period, three earthquakes with high-quality waveforms were recorded: **M** 3.7 Los Vilos (onshore), **M** 2.7 Valparaíso (offshore), and **M** 3.3 La Ligua (offshore) earthquakes (Fig. 1b–d). Despite their relatively small magnitudes, these events exhibit clear *P*- and *S*-wave waveforms, providing a valuable opportunity to evaluate how DAS techniques can benefit EEW systems.

Data, Methods, and Results

The DAS array comprises 8960 channels (i.e., sampled positions along the optical fiber cable) with a spatial sampling of 5 m and gauge length of 10 m. We downsample the data to 100 Hz, convert the raw strain data into strain rate to remove instrumental drifts, and apply a band-pass filter of [0.05, 20] Hz to suppress oceanic noises. The processed

waveforms exhibit clear *P*- and *S*-wave arrivals, as illustrated in Figure 1b-d.

Because the cable was not deployed explicitly for seismic sensing purposes, some calibration is required. In particular, the DAS interrogator (manufactured by Aragon Photonics) was placed in an electromagnetically shielded room without a Global Positioning System signal, accumulating clock errors. We calibrate the data using the theoretical travel time combined with the absolute timestamp from a nearby seismic station, C1.VA01. Using the catalog location of the monitored seismic events, we employ the 1D global velocity model IASP91 (Kennett and Engdahl, 1991) to estimate the theoretical arrival time. We observe consistent matches of both *P* and *S* waves for most DAS channels (Fig. 1b-d) with a channelinvariant time shift, accounting for the time drift (Los Vilos: 9 s, Valparaíso: 9 s, La Ligua: 12.5 s). For DAS channels beyond 7000, we notice systematic delays of 1-2 s in phase arrivals. Several factors can contribute to such delays, including uncertainties in submarine channel locations (i.e., cable positioning) in deeper ocean areas or local structure anomalies. More information is required to understand these phase delays. Thus, we only use the first 7000 channels in this work.

The first steps of EEW workflow involve detecting and locating an earthquake and rapidly determining its magnitude. In this study, we focus on evaluating the independent performance of DAS data within this EEW workflow. We have not included scenarios for which island seismic stations can collaborate with DAS for simplicity. Further conversion from the earthquake information to EEW user-side information, such as shaking intensity or ground-motion prediction, is left for future work.

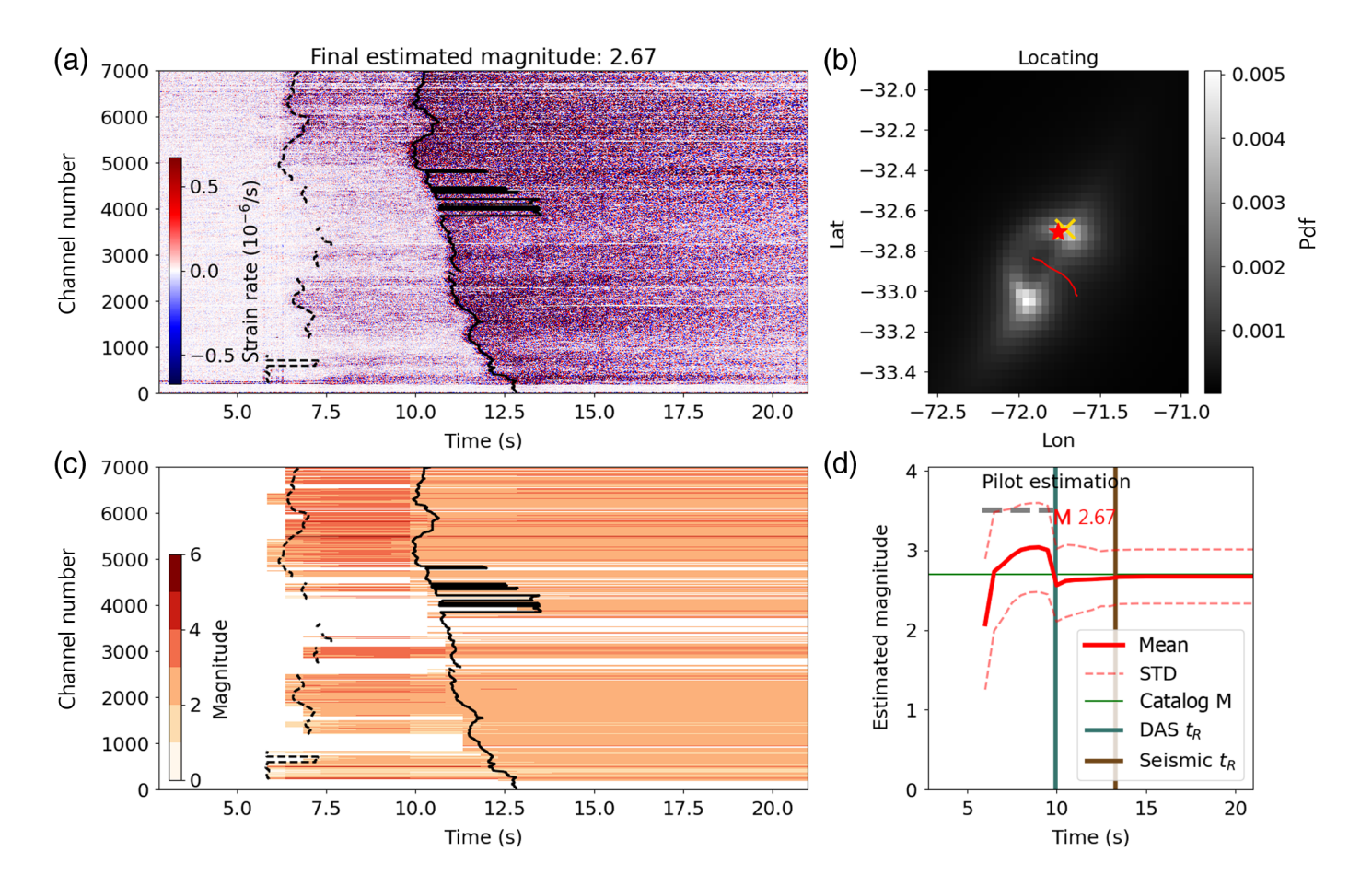
Event detection and location

Fast and accurate detection and picking of seismic phase arrivals are crucial for an effective EEW system. We employ a deep learning model, PhaseNet-DAS (Yin et al., 2023; Zhu et al., 2023), to achieve this. PhaseNet-DAS is based on self-supervised learning to transfer deep learning models from seismic datasets to DAS data (Zhu and Beroza, 2019), capable of directly processing 2D spatial-temporal DAS data with high accuracy in detection and picking. We apply the pretrained PhaseNet-DAS model (Yin et al., 2023; Zhu et al., 2023) to automatically pick the P- and S-wave arrivals for our DAS earthquake data (black lines in Fig. 1b-d). For validation, we demonstrate that picks from PhaseNet-DAS are consistent with the theoretical ones based on the global velocity model

(green lines in Fig. 1b-d). PhaseNet-DAS is efficient: processing 2 hr of data from this array takes only 10 min with one graphical processing unit (Table S1, available in the supplemental material to this article). PhaseNet-DAS's accuracy and efficiency enable real-time event detection and picking from DAS data.

Next, we employ a grid-search-based method to locate the earthquakes using the arrival times from the phase picks. We mesh the area surrounding the DAS array into location grids and precalculate the theoretical travel time from each grid point to the given DAS array based on the IASP91 velocity model (Kennett and Engdahl, 1991). We assume a source depth of 20 km for the Chile region, approximately the average depth of shallow thrust events in this area based on the Global Centroid Moment Tensor catalog (Ekström et al., 2012), to reduce computation time. Earthquakes can be rapidly located by fitting the theoretical travel time with the arrival time from phase picking. We do not explicitly search for the origin time of earthquakes; instead, we directly use the theoretical travel time from the best-fit event locations to shift the measured arrival timestamp and finally take the median as the origin time of the two offshore earthquakes analyzed. This approach enables us to fully utilize the array nature of DAS measurements to avoid an extra search in the origin time dimension and save more time for locating events. We compare the estimated origin time with the catalog origin time for the two earthquakes, finding errors as 0.30 s for the M 3.3 La Ligua event and 1.49 s for the M 2.7 Valparaíso event. We also tested depths of 10 and 30 km, and 20 km appears to be the best one to match the catalog location (Figs. S1-S6).

We search within a $3^{\circ} \times 3^{\circ}$ region with a grid size of $0.04^{\circ} \times$ 0.04° . PhaseNet-DAS provides the arrival time of both P and Swaves, which can be used to locate earthquakes. Ideally, P-wave picking is preferred for EEW; however, the DAS array in this study is nearly linear. For this simple geometry, a single seismic phase can only constrain the azimuth of an earthquake. Consequently, we fit the demeaned P-wave arrival together with the absolute difference between P- and S-wave arrival times, which corresponds to the distance from the source to each channel along the array. Taking the Valparaíso event for instance (Fig. 2a), the P and S arrivals appear to almost parallel to each other in the deep section of the cable (i.e., 5000-7000), implying the almost equidistance from the earthquake to this section of the cable. Once the distance increases along the cable toward land, the P and S arrivals separate from each other. This interesting pattern has been verified by the



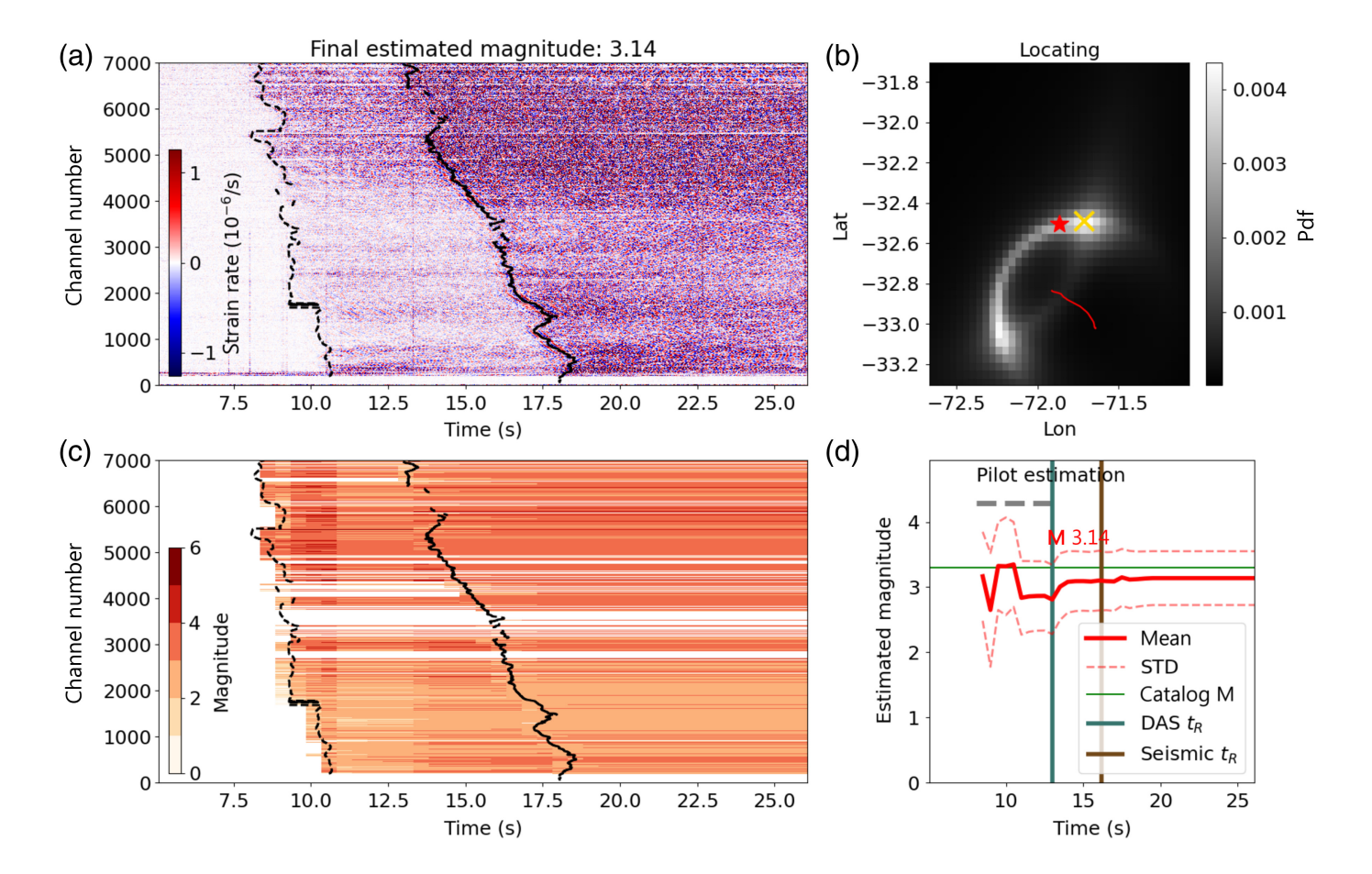
consistency between the event catalog location and our result (Fig. 2b). The array nature of DAS yields a much more accurate earthquake location. However, limited by the linear geometry of the DAS array and the 1D velocity model for the grid search, we still obtain a symmetric probability distribution with two peak probability locations (Fig. 2 and Fig. S7, Fig. 3 and Fig. S8, and supplemental movies). We also used another dedicated method to estimate earthquake locations, based on beamforming and a modified triangulation approach (Muñoz and Soto, 2022), but obtained similar estimations and ambiguity in earthquake locations. This limitation can be improved by using multiple DAS arrays with more complex array geometries in the future.

Earthquake magnitude estimation

Given the event detection and location, the next step is to estimate the earthquake magnitude. Using DAS for EEW presents a major challenge in this regard. Direct use of DAS amplitude information is often limited by unknown cable coupling (Ajo-Franklin *et al.*, 2019; Trainor-Guitton *et al.*, 2019; Lindsey *et al.*, 2020; Paitz *et al.*, 2020) and uncertain instrumental

Figure 2. DAS-earthquake early warning (EEW) results of the M 2.7 Valparaíso earthquake at one location. Results from the other symmetric location are shown in Figure S7. (a) The DAS waveforms with the phasepicking in black lines. (b) The location results from the grid search. The background image is the probability density distribution converted from the L1-norm data misfit of both P-wave arrival time and difference of Pand S-wave arrival time. Red line shows the DAS array. Red star and yellow cross indicate the catalog location and one best-fit location, respectively. (c) The corresponding magnitude estimation based on the peak DAS amplitude for each channel. (d) The magnitude estimation from taking median of all available channels, shown by the red line. The red dashed lines indicate the standard deviation of magnitude estimation from channels. The green horizontal lines indicate the catalog magnitude for reference. A gray dashed line indicates the pilot estimation period. Dark green and brown lines correspond to the defined response time t^R s of DAS array and seismic station, respectively.

response (Lindsey et al., 2020; Paitz et al., 2020). To overcome these limitations, Yin et al. (2023) propose a data-based scaling relation between the DAS peak amplitude and earthquake magnitude. The scaling relations incorporate the calibration of site effects at individual channel locations and have been



shown to be transferable from one study area to another with minor calibrations (Yin et al., 2023).

This study uses the scaling relation from Yin *et al.* (2023) to estimate the earthquake magnitude from DAS amplitude:

$$\log_{10} E_i^P = 0.437M - 1.269 \log_{10} D_i + K_i^P, \tag{1}$$

$$\log_{10} E_i^{S} = 0.690M - 1.588 \log_{10} D_i + K_i^{S}, \tag{2}$$

in which E is the observed peak amplitude of the DAS strain rate, D is the hypocentral distance in kilometers to each DAS channel, and M is the earthquake catalog magnitude. The subscript i corresponds to each channel. P and S waves have different scaling coefficients.

We take the **M** 3.7 land earthquake near Los Vilos (Fig. 1a), and measure its peak DAS amplitude for both P and S waves. The measured peak amplitude, the catalog magnitude, and location are substituted into equations (1) and (2) to get the site calibration terms of the DAS array K_i at available channels (Fig. S9).

We apply the transferred scaling relation to the two offshore earthquakes to estimate their magnitude. We first estimate the

Figure 3. Results of the **M** 3.3 La Ligua earthquake. (a) The DAS waveforms with the phase picking. (b) The location results from the grid search. (c) The corresponding magnitude estimation based on the peak DAS amplitude for each channel. (d) The magnitude estimation from taking median of all available channels. Symbols are the same as Figure 2. Results from the other symmetric location are shown in Figure S8.

magnitude at each channel and then take the median value of all available channels as the final magnitude estimation. The magnitude of the M 2.7 Valparaíso earthquake is estimated as 2.6 and 2.7 with P and S waves, respectively. The magnitude of the M 3.3 La Ligua earthquake is estimated as 3.2 and 2.9 with P and S waves, respectively. Our estimated magnitude is consistent with the catalog magnitude with an error of less than 0.5 unit of magnitude (Fig. S10). The transferred scaling relations can provide reliable magnitude estimation. We can expect that the use of more events can further improve the site term calibration and the accuracy of magnitude estimation.

A potential workflow for point-source DAS-EEW

Because we have all the necessary components for point-source EEW with a DAS array, we propose a workflow that incorporates DAS as an additional EEW system. The data stream is first processed through a conversion and filtering preprocessor, and then an automatic phase-picker, such as PhaseNet-DAS or other similar methods, is run for event detection. Upon detecting an event, its phase picks and peak amplitudes are recorded for subsequent location and magnitude estimations. Here, we simulate the streaming with real data and take the measurements of phase picks from PhaseNet-DAS and the peak amplitude. These idealized experiments allow us to assess the proposed workflow's integrated uncertainties and overall performance.

We specifically test the two offshore earthquakes (Figs. 2, 3). Using the method introduced in the Event detection and location section, we locate the earthquakes based on the available phase picks at the time of streamed data. The locations and peak DAS amplitudes are then used in the transferred scaling relations (equations 1, 2) in the Earthquake magnitude estimation section to estimate the earthquake magnitude. This workflow offers real-time earthquake location and magnitude estimation for EEW (supplemental movies). In this study, we update the measurements every 0.5 s; however, the update frequency can be adjusted based on specific situations.

As mentioned in the Event Detection and Location section, the linear DAS array cannot accurately determine the earthquake location with a single seismic phase. We refer to the estimation between the P arrival and the S arrival as the pilot estimation. During the pilot estimation, we determine the most likely location of the earthquake within an assumed maximum distance to provide a rapid first-order estimation for reference. In our demonstration, we assume the maximum distance *D* to be 50 km (Figs. 2, 3d), and we have tested other values as well. As the *S* wave is detected, the distance between the earthquake and the array can be accurately determined using measurements from only a few DAS channels (supplemental movies). From this point, the magnitude estimation is reliable enough for further decision making. Because of the location ambiguity, we still have two possible event locations, and we have to keep both in this experiment. This issue can be easily fixed, as discussed before. The estimation process concludes 2 s after the last *S* arrival detected by the DAS array.

We compare the final results with the catalog information of these two events (Figs. 2, 3). We find that the distance from the two events to the array can be accurately measured; however, the absolute locations of earthquakes have an ambiguity of two symmetric locations due to the linearity of the array. The magnitude estimation is accurate for both the events.

Once the *S* wave is detected after the pilot estimation period, the magnitude can be determined within 2 s, and the final error is less than 0.2. We also try downsampling the data by taking one of every 50 channels and applying the same workflow. The downsampling can further accelerate the workflow, and the results look almost the same (Figs. S11, S12). These examples demonstrate the feasibility of using the DAS array for EEW, particularly for offshore earthquakes.

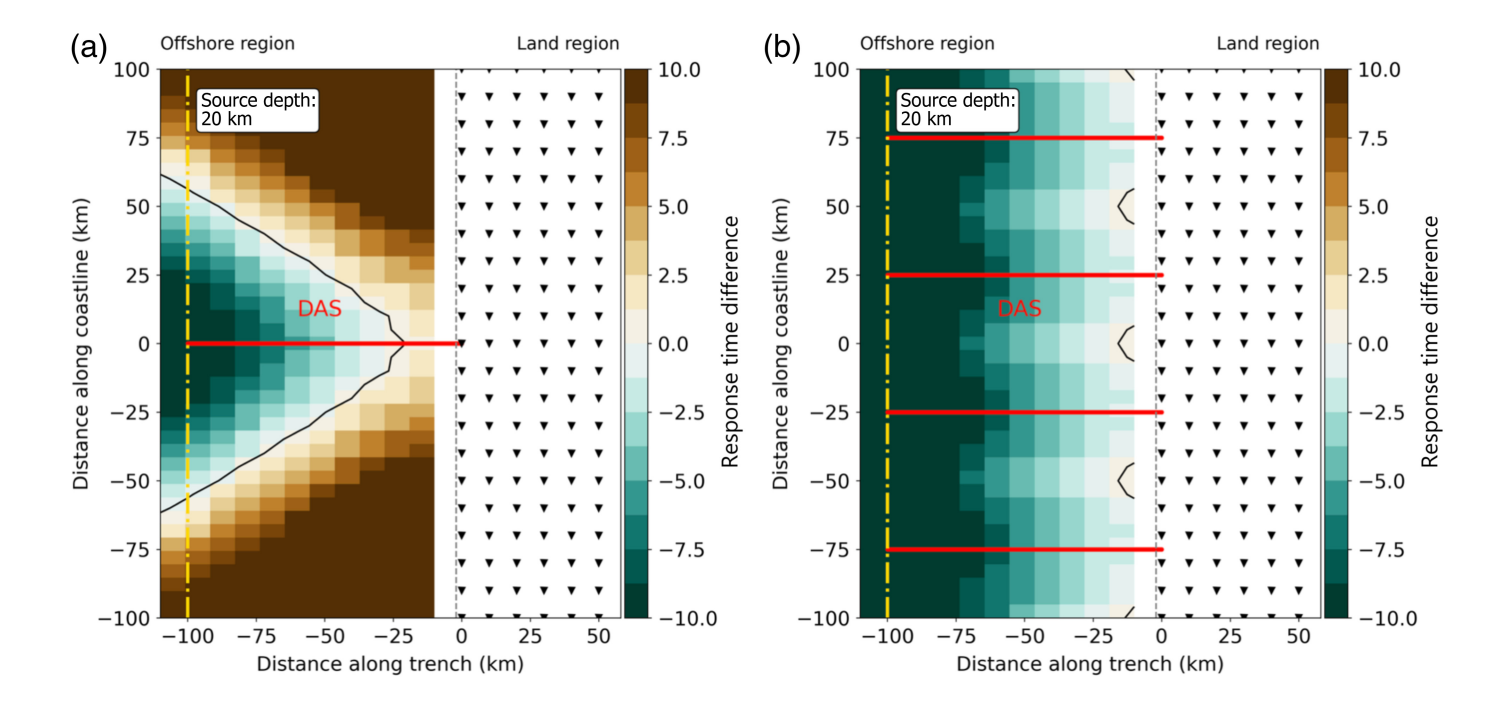
Discussion

Comparison with current seismic EEW systems

Effective EEW systems require long-term deployments of seismic sensors in high-risk regions. However, offshore seismometers are extremely costly to deploy and maintain. DAS, which can directly utilize existing submarine cables, offers an economical approach to extending the EEW system for offshore earthquakes. Currently, there are 487 global cables and 1304 landing cable nodes (numbers from Telegeography: see Data and Resources), so there is a potential to enable 1300+ arrays with 7000+ channels, resulting in nearly 10 million offshore seismometers without additional deployment.

Our results demonstrate the feasibility of offshore DAS-EEW. To further estimate the potential improvements DAS-EEW could provide over current systems based on land seismometers, we compare the response time t_R of a current system and another based on DAS technology. This time is defined as the earliest time when an EEW system can start alerting after the occurrence of an earthquake. We focus on the comparison between a land EEW system (system 1) based on the point-source method (e.g., EPIC, Allen, 2007; Allen and Melgar, 2019; Chung et al., 2020) and an offshore DAS system (system 2). For simplicity, we ignore the time required for data transmission and telemetry in both the systems. The response time t_R^1 of system 1 is the time when the *P* wave is measured on four onshore stations, assuming that all of them are triggered (Chung et al., 2020). Based on our previous discussion, the response time t_R^2 of system 2 can be approximated as the earliest S-wave arrival time at a single DAS array channel. For the two offshore earthquakes in this study, we calculate t_R^1 using the permanent seismic stations (Fig. 1a) and t_R^2 for the DAS array. Our results indicate that the DAS array can provide about 3 s earlier response time than the land seismic stations (Figs. 2d, 3d).

Next, we systematically compare t_R^1 and t_R^2 by calculating the response time for a synthetic domain generalized for an offshore region. Offshore earthquakes can occur at any point



between the coastline and the trench (Fig. 4). The trench is set at 100 km from the coastline, based on the Cascadia and Chile subduction zones. For system 1, we assume that seismic stations are uniformly deployed on land with 10 km spacing. For system 2, we set a 100 km long linear DAS array starting from the coastline. We then assume an earthquake depth of 20 km, and use the IASP91 global velocity model to calculate the corresponding t_R^1 and t_R^2 . We use $\Delta t_R = t_R^2 - t_R^1$ to evaluate both systems: if Δt_R is negative, it means that the DAS system can provide extra alert time. Our results show that a simple linear DAS array can provide over 5 s more in a 2500 km² (= $100 \times 50/2 \text{ km}^2$) triangular area near the trench (Fig. 4a).

Having more DAS arrays can significantly improve the system. For instance, multiple DAS arrays can locate earthquakes with only P-wave arrival time and provide an even earlier alert time. To demonstrate this, we designed another synthetic case with multiple DAS arrays spaced 50 km apart and working together (Fig. 4b). With the P-wave arrival time of the DAS t_R^2 , the system can cover almost the entire offshore area, providing several more seconds of alert time. The extra response time is significant for EEW systems to reduce human injury and property loss (Strauss and Allen, 2016), particularly for coastal cities with high population density.

Outlook and future work for DAS-EEW

The two offshore earthquakes investigated in this study, although of small magnitude and nondamaging, allowed us to assess the

Figure 4. Response time difference $\Delta t_R = t_R^2 - t_R^1$ of our synthetic offshore domain (a) single DAS array system. (b) Multiple DAS arrays system. DAS arrays are shown by the red lines. Triangles are the land seismic stations with 10 km spacing. Δt_R in the offshore region is indicated by the color image. Thin gray dashed line and yellow dotted line are the coastline and trench, respectively. Black contours also indicate the point with $\Delta t_R = 0$.

DAS technique's feasibility for EEW in offshore areas. We developed a point-source-based workflow for using DAS in EEW, covering detection, location, and magnitude estimation.

Three primary noise sources were identified in our dataset: (1) weak *P*-wave amplitude, particularly in channels 2000–5000 (Fig. 1); (2) potential secondary arrivals stronger than the initial *P* wave; and (3) inaccurate cable geometry in deep water. Despite these challenges, our EEW method still offers reliable location and magnitude estimates even with relatively low-quality data, demonstrating that a single array can enhance offshore EEW systems using DAS. Furthermore, the DAS technique simplifies instrument deployment, requiring only a connection to a submarine cable at the landing station, centralizing all data processing. Its recent extension into the L-band part of the spectrum allows integration with existing submarine cables without interference. Developing the necessary software and hardware will likely involve extensive interdisciplinary collaboration.

Our evaluation also highlights several areas for future work in DAS-EEW. Although all current steps are computationally

efficient in principle, we have not yet systematically tested the time required for each step. A realistic replay test would provide better insight into the actual time required, and we leave this as an ongoing task. Our evaluation is based on the point-source EEW algorithm (Chung et al., 2019), which may saturate in magnitude estimation for very large earthquakes. As a result, it is crucial to investigate how DAS results become saturated when DAS data for larger M6+ earthquakes becomes available. Developing innovative unsaturated methods for DAS, similar to finite-fault-based methods such as FinDer (Böse et al., 2012), could be beneficial. Moreover, we only consider DAS as an independent system in this study. Exploring how to implement DAS within existing EEW systems using various methods is another critical direction for the future research.

Conclusion

We present a real-data demonstration for offshore DAS-EEW. With seismic signals from an offshore DAS array in Chile, we detect earthquakes, obtain phase picks to constrain locations, and further apply a transferred scaling relation for robust magnitude estimations. We test the EEW workflow on two offshore earthquakes. Our results show that submarine DAS systems can improve alert times and serve as an economical and effective complement to EEW systems, particularly for enhancing coverage in offshore regions.

Data and Resources

The proprietary distributed acoustic sensing (DAS) data were from an undisclosed source and cannot be released to the public. The supplemental material includes additional figures for locating events, site calibration terms, and magnitude estimation. The Python codes of this study are available on GitHub at https://github.com/yinjiuxun/DAS-EEW-offshore (last accessed October 2023). The information about Submarine Cable Map is available at https://www.submarinecablemap.com/ (last accessed May 2023).

Declaration of Competing Interests

The authors acknowledge that there are no conflicts of interest recorded.

Acknowledgments

The authors are grateful for the constructive suggestions and discussions from the anonymous reviewers to improve the article. The authors also thank Aragon Photonics for providing the distributed acoustic sensing (DAS) interrogator used in this

work and Eduardo Saravia for helping with the experimental test. This work was supported by the Office of Emergency Services, State of California, under MCG.CEEWS3-1-CALIFOES.NEWS, funding source Award Number 6113-2019, the Moore Foundation, National Science Foundation (NSF) CAREER Award 1848166, and U.S. Geological Survey (USGS) Grant Number G23AP00111. This work was also supported by Chilean National Agency for Research and Development under Projects FONDECYT Regular 1200299, FONDEF IDeA I+D ID20I10089, and Basal FB0008.

References

- Ajo-Franklin, J. B., S. Dou, N. J. Lindsey, I. Monga, C. Tracy, M. Robertson, V. Rodriguez Tribaldos, C. Ulrich, B. Freifeld, T. Daley, and X. Li (2019). Distributed acoustic sensing using dark fiber for near-surface characterization and broadband seismic event detection, Sci. Rep. 9, no. 1, 1328.
- Allen, R. M. (2007). The ElarmS earthquake early warning methodology and application across California, in *Earthquake Early Warning Systems*, P. Gasparini, G. Manfredi, and J. Zschau (Editors), Springer, Berlin, Heidelberg, 21–43.
- Allen, R. M., and D. Melgar (2019). Earthquake early warning: Advances, scientific challenges, and societal needs, *Annu. Rev. Earth Planet. Sci.* **47**, no. 1, 361–388, available at https://doi.org/10.1146/annurev-earth-053018-060457 (last accessed October 2023).
- Böse, M., C. Felizardo, and T. H. Heaton (2015). Finite-Fault Rupture Detector (FinDer): Going real-time in Californian ShakeAlert Warning System, *Seismol. Res. Lett.* **86**, no. 6, 1692–1704.
- Böse, M., T. H. Heaton, and E. Hauksson (2012). Real-time Finite Fault Rupture Detector (FinDer) for large earthquakes, *Geophys. J. Int.* **191**, no. 2, 803–812.
- Chung, A. I., I. Henson, and R. M. Allen (2019). Optimizing earth-quake early warning performance: ElarmS-3, *Seismol. Res. Lett.* **90**, no. 2A, 727–743.
- Chung, A. I., M. Meier, J. Andrews, M. Böse, B. W. Crowell, J. J. McGuire, and D. E. Smith (2020). ShakeAlert earthquake early warning system performance during the 2019 Ridgecrest earthquake sequence, *Bull. Seismol. Soc. Am.* **110**, no. 4, 1904–1923.
- Ekström, G., M. Nettles, and A. M. Dziewoński (2012). The global CMT project 2004–2010: Centroid-moment tensors for 13,017 earthquakes, *Phys. Earth Planet. In.* **200/201**, 1–9.
- Kennett, B. L. N., and E. R. Engdahl (1991). Traveltimes for global earthquake location and phase identification, *Geophys. J. Int.* **105**, no. 2, 429–465.
- Kohler, M. D., E. S. Cochran, D. Given, S. Guiwits, D. Neuhauser, I.
 Henson, R. Hartog, P. Bodin, V. Kress, S. Thompson, *et al.* (2017).
 Earthquake early warning ShakeAlert system: West coast wide production prototype, *Seismol. Res. Lett.* 89, no. 1, 99–107.
- Kohler, M. D., D. E. Smith, J. Andrews, A. I. Chung, R. Hartog, I. Henson, D. D. Given, R. de Groot, and S. Guiwits (2020).

- Earthquake early warning ShakeAlert 2.0: Public rollout, *Seismol. Res. Lett.* **91,** no. 4, 1763–1775.
- Lindsey, N. J., E. R. Martin, D. S. Dreger, B. Freifeld, S. Cole, S. R. James, B. L. Biondi, and J. B. Ajo-Franklin (2017). Fiber-optic network observations of earthquake wavefields, *Geophys. Res. Lett.* 44, no. 23, 11,792–11,799, doi: 10.1002/2017GL075722.
- Lindsey, N. J., H. Rademacher, and J. B. Ajo-Franklin (2020). On the broadband instrument response of fiber-optic DAS arrays, *J. Geophys. Res.* **125**, no. 2, e2019JB018145, doi: 10.1029/2019JB018145.
- Lior, I., D. Rivet, J.-P. Ampuero, A. Sladen, S. Barrientos, R. Sánchez-Olavarría, G. A. Villarroel Opazo, and J. A. Bustamante Prado (2023). Magnitude estimation and ground motion prediction to harness fiber optic distributed acoustic sensing for earthquake early warning, Sci. Rep. 13, no. 1, 424.
- Marra, G., D. M. Fairweather, V. Kamalov, P. Gaynor, M. Cantono, S. Mulholland, B. Baptie, J. C. Castellanos, G. Vagenas, J.-O. Gaudron, et al. (2022). Optical interferometry-based array of seafloor environmental sensors using a transoceanic submarine cable, Science 376, no. 6595, 874–879.
- Muñoz, F., and M. A. Soto (2022). Enhancing fibre-optic distributed acoustic sensing capabilities with blind near-field array signal processing, *Nat. Comm.* **13**, no. 1, 4019.
- Paitz, P., P. Edme, D. Gräff, F. Walter, J. Doetsch, A. Chalari, C. Schmelzbach, and A. Fichtner (2020). Empirical investigations of the instrument response for distributed acoustic sensing (DAS) across 17 Octaves, Bull. Seismol. Soc. Am. 111, no. 1, 1–10.
- Satake, K., and B. F. Atwater (2007). Long-term perspectives on giant earthquakes and tsunamis at subduction zones, *Annu. Rev. Earth Planet. Sci.* **35**, 349–374.

- Satake, K., K. Shimazaki, Y. Tsuji, and K. Ueda (1996). Time and size of a giant earthquake in Cascadia inferred from Japanese tsunami records of January 1700, *Nature* **379**, no. 6562, 246–249.
- Shinohara, M., T. Yamada, T. Akuhara, K. Mochizuki, and S. Sakai (2022). Performance of seismic observation by distributed acoustic sensing technology using a seafloor cable off Sanriku, Japan, *Frontiers Mar. Sci.* 466.
- Strauss, J. A., and R. M. Allen (2016). Benefits and costs of earthquake early warning, *Seismol. Res. Lett.* **87**, no. 4, 765–772.
- Trainor-Guitton, W., A. Guitton, S. Jreij, H. Powers, and B. Sullivan (2019). 3D imaging of geothermal faults from a vertical DAS fiber at Brady Hot Spring, NV USA, *Energies* **12**, no. 7, 1401.
- Yin, J., W. Zhu, J. Li, E. Biondi, Y. Miao, Z. J. Spica, L. Viens, M. Shinohara, S. Ide, K. Mochizuki, et al. (2023). Earthquake magnitude with DAS: A transferable data-based scaling relation, Geophys. Res. Lett. 50, no. 10, e2023GL103045.
- Zhan, Z. (2019). Distributed acoustic sensing turns fiber-optic cables into sensitive seismic antennas, *Seismol. Res. Lett.* **91**, no. 1, 1–15.
- Zhu, W., and G. C. Beroza (2019). Phasenet: A deep-neural-network-based seismic arrival-time picking method, *Geophys. J. Int.* **216**, no. 1, 261–273.
- Zhu, W., E. Biondi, J. Li, J. Yin, Z. E. Ross, and Z. Zhan (2023). Seismic arrival-time picking on distributed acoustic sensing data using semi-supervised learning, arXiv preprint, available at https://arxiv.org/abs/2302.08747 (last accessed October 2023).

Manuscript received 5 May 2023 Published online 12 October 2023